Surface Electrochemistry of CO on Reconstructed Gold Single Crystal Surfaces Studied by Infrared Reflection Absorption Spectroscopy and Rotating Disk Electrode

ARTICLE *in* JOURNAL OF THE AMERICAN CHEMICAL SOCIETY · AUGUST 2004

Impact Factor: 12.11 · DOI: 10.1021/ja049038s · Source: PubMed

4 AUTHORS:

Berislav B. Blizanac
Cabot Corporation
33 PUBLICATIONS **1,984** CITATIONS
SEE PROFILE

Matthias Arenz
University of Copenhagen
90 PUBLICATIONS **4,457** CITATIONS
SEE PROFILE

Philip N Ross
University of California, Berkeley
361 PUBLICATIONS **21,519** CITATIONS
SEE PROFILE

N. M. Marković
Argonne National Laboratory
285 PUBLICATIONS **22,036** CITATIONS
SEE PROFILE

J|A|C|S
ARTICLES
Published on Web 07/27/2004

Surface Electrochemistry of CO on Reconstructed Gold Single Crystal Surfaces Studied by Infrared Reflection Absorption Spectroscopy and Rotating Disk Electrode

Berislav B. Blizanac, Matthias Arenz, Philip N. Ross, and Nenad M. Marković*

Contribution from the Materials Sciences Division Lawrence Berkeley National Laboratory, University of California, Berkeley, California 94720

Received February 20, 2004; E-mail: nmmarkovic@lbl.gov

Abstract: The electrooxidation of CO has been studied on reconstructed gold single-crystal surfaces by a combination of electrochemical (EC) and infrared reflection absorption spectroscopy (IRAS) measurements. Emphasis is placed on relating the vibrational properties of the CO adlayer to the voltammetric and other macroscopic electrochemical responses, including rotating disk electrode measurements of the catalytic activity. The IRAS data show that the C−O stretching frequencies are strongly dependent on the surface orientation and can be observed in the range 1940−1990 cm^{-1} for the 3-fold bridging, 2005−2070 cm^{-1} for the 2-fold bridging, and 2115−2140 for the terminal position. The most complex CO spectra are found for the Au(110)-(1 × 2) surface, i.e., a band near 1965 cm^{-1}, with the second, weaker band shifted positively by about 45 cm^{-1} and, finally, a weak band near 2115 cm^{-1}. While the C−O stretching frequencies for a CO adlayer adsorbed on Au(111)-(1 × 23) show ν_{CO} bands at 2029−2069 cm^{-1} and at 1944−1986 cm^{-1}, on the Au(100)-"hex" surface a single CO band is observed at 2004−2029 cm^{-1}. In the "argon-purged" solution, the terminal ν_{co} band on Au(110)-(1 × 2) and the 3-fold bridging band on the Au(111)-(1 × 23) disappear entirely. The IRAS/EC data show that the kinetics of CO oxidation are structure sensitive; i.e., the onset of CO oxidation increases in the order Au(110)-(1 × 2) ≥ Au(100)-"hex" > Au(111)-(1 × 23). Possible explanations for the structure sensitivity are discussed.

1. Introduction

The surface (electro)chemistry of CO adsorbed on transition metal surfaces has been the subject of intense theoretical and experimental studies; for an overview see refs 1−4. Carbon monoxide adsorption is of interest for several reasons, including (i) the search for CO tolerant catalysts or catalysts with an intrinsically high catalytic activity for the oxidation of hydrogen in the presence of trace levels of carbon monoxide[5,6] and (ii) the elucidation of its role as an adsorbed poison for the electrooxidation of organic molecules on monometallic and bimetallic electrodes.[2,7,8] The best CO-tolerant catalysts reported so far are created by alloying Pt with an ad-metal which is capable simultaneously to activate water (and thus to oxidize CO) at more negative potentials than Pt and to alter the electronic properties of Pt so that the energy of adsorption of CO is significantly reduced relative to the clean Pt metal.[6,9,10] As a consequence, the adsorption and electrooxidation of CO on Pt and Pt-bimetallic surfaces have occupied for a long time a special place in surface electrochemistry. In the last three years, however, in an attempt to find a cost-effective replacement of Pt, CO oxidation and the oxidation of CO/H_2 mixtures were investigated on AuPd bimetallic alloys.[11] The combination of Au and Pd was chosen because Pd is as good as Pt for the hydrogen oxidation reaction[6] and because Au is a superior CO oxidation catalyst.[12−16] In contrast to Pt, for the Au-based catalysts there is still much to be understood regarding the adsorptive chemistry as well as the electrocatalytic properties of CO at the molecular level. In fact, results for the interaction of CO with either a polycrystalline Au electrode[17−19] or Au single-crystal electrodes[13,14,16,20] are scarce.

(1) Markovic, N. M.; Ross, P. N. *Surf. Sci. Rep.* **2002**, *45*, 121−254.
(2) Waszczuk, P.; Lu, G.; Wieckowski, A.; Lu, C.; Rice, C.; Masel, R. I. *Electrochim. Acta* **2002**, *47*, 3637−3652.
(3) Park, S.; Wasileski, S. A.; Weaver, M. J. *Electrochim. Acta* **2002**, *47*, 3611−3620.
(4) Shubina, T. E. *Electrochim. Acta* **2002**, *47*, 3621−3628.
(5) Gasteiger, H. A.; Markovic, N.; Ross, P. N. *J. Phys. Chem.* **1995**, *99*, 16757−16767.
(6) Markovic, N. M. The hydrogen electrode reaction and the electrooxidation of CO and H_2/CO mixtures on well-characterized Pt and Pt-bimetallic surfaces. Vielstich, W., Lamm. A, Gasteiger, H. A., Eds. [volume 2 Electrocatalysis]; 368−393. 2003. John Wiley & Sons Inc. Handbook of Fuel Cells; Fundamentals, Technology and Application. Ref Type: Serial (Book, Monograph).
(7) Hamnett, A.; Weeks, S. A.; Kennedy, B. J.; Troughton, G.; Christensen, P. A. *Ber. Bunsen-Ges. Phys. Chem.* **1990**, *94*, 1014−1020.
(8) Jarvi T. D.; Stuve, E. M. *Electrocatalysis*; Wiley-VCH: New York, 1998; Chapter 3, pp 75−153.
(9) Watanabe, M.; Motoo, S. *J. Electroanal. Chem.* **1975**, *60*, 275−283.
(10) Ross, P. N., Jr. *Electrocatalysis*; Wiley-VCH: New York, 1998; Chapter 2, pp 43−74.
(11) Schmidt, T. J.; Stamenkovic, V.; Markovic, N. M.; Ross, P. N. *Electrochim. Acta* **2003**, *48*, 3823−3828.
(12) Kita, H.; Nakajima, H.; Hayashi, K. *J. Electroanal. Chem.* **1985**, *190*, 141−156.
(13) Chang, S.-L.; Hamelin, A.; Weaver, M. J. *Surf. Sci. Lett.* **1990**, *239*, L543−L547.
(14) Chang, S.-L.; Hamelin, A.; Weaver, M. J. *J. Phys. Chem.* **1991**, *95*, 5560−5567.
(15) Edens, G. J.; Hamelin, A.; Weaver, M. J. *J. Phys. Chem.* **1996**, *100*, 2322−2329.
(16) Blizanac, B. B.; Lucas, C.; Gallagher, M.; Arenz, M.; Ross, P. N.; Markovic, N. M. *J. Phys. Chem.* **2003**, *108*, 625−634.

10.1021/ja049038s CCC: $27.50

Fundamental insight into the surface chemistry of CO adsorption on gold single-crystal surfaces in an electrochemical environment was initially obtained by a combination of linear sweep voltammetry and surface infrared spectroscopy.[13,14] However, the level of interpretation of these EC/IRAS results was limited by several factors: (i) the lack of in situ characterization of the effects of CO on surface reconstruction (i.e., arrangements of metal surface atoms which differ from the ideal bulk-termination structure) and surface relaxation (i.e., the case in which the surface layer has the same structure as the underlying bulk crystal but the layer is displaced along the surface normal direction from the position expected for bulk termination of the crystal lattice); (ii) a weak infrared band intensity of CO adsorbed on Au; and (iii) the lack of controlled transport of CO from the bulk of the solution to the Au surface. Very recently, however, it was reported that in acid solution the "reconstructed" ↔ unreconstructed phase transition on the Au(*hkl*) is not affected by the adsorption of CO.[16] As a consequence, the adsorption/oxidation chemistry of CO can be studied on the thermodynamically stable surface.

In this paper, we present a study of the relationship between the macroscopic electrochemical kinetic rate of CO electrooxidation and the molecular-level information on the bond coordination of adsorbed CO on *reconstructed* Au low-index single-crystal surfaces. For simplicity, the reconstructed surfaces of Au(100), Au(111) and Au(110) will in the following be denoted as Au(100)-"hex", Au(111)−(1 × 23) and Au(110)−(1 × 2), respectively. The unreconstructed surfaces, on the other hand, will be denoted simply as (1 × 1). Information about the preferred binding site geometry of CO on Au single-crystal electrodes is established by means of infrared reflection−absorption spectroscopy. While the interpretation of the spectra from the Au(*hkl*)-CO systems is of major focus here, the evolution of the CO_2 stretching band during CO electrooxidation is monitored as well, providing an independent measurement of the oxidative removal of CO from Au surfaces.

2. Experimental Section

2.1. Electrochemical Measurements. The pretreatment and assembly of the Au single-crystal surfaces (0.283 cm^2) into an RDE configuration was described previously;[21] e.g., the crystals were flame annealed in a propane flame and cooled in an Ar atmosphere before being mounted in the RDE setup. Subsequently, the electrodes were transferred to a thermostated standard three compartment electrochemical cell and immersed into the Ar-purged electrolyte at ∼298 K (Ar: Bay Gas Research Purity; 0.1 M $HClO_4$ Aldrich Semiconductor Grade prepared with triply pyrodistilled water) under potentiostatic control at ∼−0.05 V. Prior to the CO measurements, a cyclic voltammogram was recorded in order to confirm the cleanliness of the electrode surface. Subsequently, the solution was saturated with CO for at least 10 min (Matheson, Matheson Grade, 4 N) at a rotation rate of 2500 rpm, to warrant the saturation of the CO adlayer. Two types of CO experiments were performed: (i) bulk oxidation in solution saturated with CO (1 atm = 10^5 Pa) and (ii) the oxidation of a saturated CO adlayer in Ar-purged solution, i.e., so-called "stripping" experiments. In both experiments, when either measuring the polarization curves for oxidation of dissolved CO at various rotation rates or recording the "stripping" curves in Ar-purged solution at 2500 rpm, the electrode potential was maintained at −0.05 V for 5 min prior to recording each positive-going sweep. The reference electrode was a saturated calomel electrode (SCE) separated by a closed electrolytic bridge from the working electrode compartment in order to avoid chloride contamination. All potentials, however, refer to that of the reversible hydrogen electrode measured on Pt in the same electrolyte.

2.2. IRAS Measurements. The in situ IRAS measurements were performed with a Nicolet Nexus 670 spectrometer purged with nitrogen and equipped with an MCT detector cooled with liquid nitrogen. As reported elsewhere,[22] all IR measurements were performed in a spectroelectrochemical glass cell designed for an external reflection mode in a thin layer configuration. The cell is coupled at its bottom with a CaF_2 prism beveled at 60° from the prism base. Closely following the electrochemical protocol, prior to each measurement a cyclic voltammogram was recorded in order to confirm the cleanliness of the electrode surface. Subsequently, while holding the electrode potential at −0.05 V, the solution was saturated with CO for at least 10 min before the thin layer configuration was established. The spectra (8 cm^{-1} resolution) were recorded either in CO-free or in CO-saturated solution. All measurements were performed using p-polarized light. To obtain a single beam spectrum, 50 scans were collected at each potential resulting in a recording time of 25 s. Absorbance spectra were calculated as the ratio $-\log(R/R_0)$, where R and R_0 are the reflectance values corresponding to the sample and reference spectra, respectively. A reference spectrum for CO was recorded at 1.5 V, where the oxidative removal of the CO adlayer is complete. For CO_2 the spectrum recorded at −0.05 V, i.e., before the onset of oxidation of the CO adlayer, was referenced to the potentials indicated. The reference potential in the spectroelectrochemical cell was controlled by an RHE.

3. Results

3.1. Adsorption of CO IRAS Measurements. 3.1.1. Au(100)-"hex". Figure 1a consists of a series of representative potential-dependent IRAS spectra, referenced to the single beam spectrum at 1.5 V of CO, adsorbed at Au(100)-"hex" in Ar-purged (red curves) and CO-saturated (blue curves) solution. At saturation coverage (−0.05 V), a very sharp C−O stretch (fwhm = 25 cm^{-1}) is observed at 2004 cm^{-1}, which shifts linearly when increasing the potential; in the insert of Figure 1, a plot of the stretching frequency ν, versus the electrode potential E, gives a slope of $d\nu/dE$ = 36 cm^{-1} V^{-1}. Further inspection of Figure 1a reveals that the same applies for the Ar-purged solution; i.e., a single band centered at 2004 cm^{-1}at negative potentials shifts linearly at a rate of about dn/dE = 40 cm^{-1} V^{-1} (insert of Figure 1) toward positive potentials. Consequently, we can conclude that for CO bulk oxidation as well as CO "stripping" only one type of adsorption site is involved and that no major change in the coordination of the CO adlayer occurs when increasing the potential. This is particularly true for the potential range below the onset of CO oxidation (E < 0.4 V), the latter being established by monitoring the concomitant development of the O−C−O stretch of dissolved CO_2 at 2343 cm^{-1}. The CO_2 band intensities, which are depicted in Figure 1b, show that the onset potential for bulk CO oxidation is shifted negatively by ca. 0.3 V with respect to the CO stripping curve, consistent with a positive reaction order with respect to the CO partial pressure. Plots of the integrated intensities of the COad (I_{CO}) and CO_2 band (I_{CO_2}) as a function

(17) Kunimatsu, K.; Aramata, A.; Nakajima, H.; Kita, H. *J. Electroanal. Chem.* **1986**, *207*, 293−307.
(18) Ikezawa, Y.; Saito, H.; Matsubayashi, H.; Toda, G. *J. Electroanal. Chem.* **1988**, *252*, 395−402.
(19) Sun, S.-G.; Cai, W.-B.; Osawa, M. *J. Phys. Chem.* **1999**, *103*, 2460−2466.
(20) Edens, G. J.; Gao, X.; Weaver, M. J.; Markovic, N. M.; Ross, P. N. *Surf. Sci. Lett.* **1994**, *302*, L275-L282.
(21) Schmidt, T. J.; Stamenkovic, V.; Arenz, M.; Markovic, N. M.; Ross, P. N. *Electrochim. Acta* **2002**, *47*, 3765−3776.
(22) Stamenkovic, V.; Arenz, M.; Lucas, C.; Gallagher, M.; Ross, P. N.; Markovic, N. M. *J. Am. Chem. Soc.* **2003**, *125*, 2736−2745.

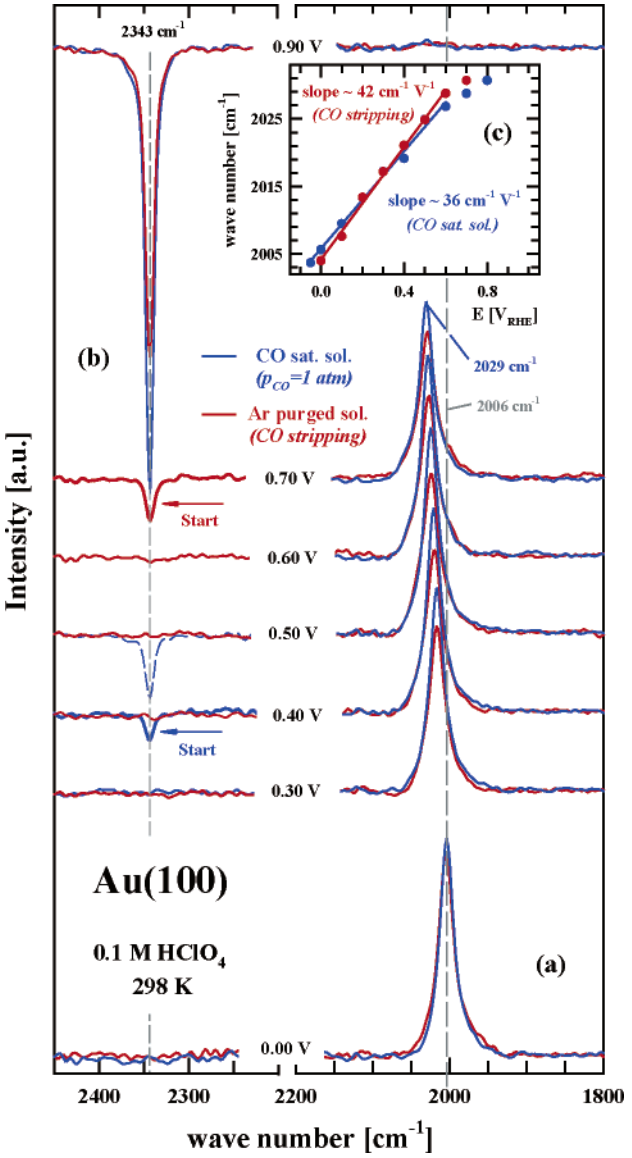

Figure 1. (a) Series of infrared spectra during progressive oxidation of CO on Au(100)-"hex" in 0.1 M $HClO_4$ solution saturated by CO (blue curves) and purged with Ar (red curves). Each spectrum is based on 50 interferometer scans accumulated at the potential indicated; notice the position of CO bands between 0.7 and 0.9 V can be discerned from the insert. (b) Series of infrared spectra for CO_2 production; note, for clarity, the CO_2 spectra between 0.7 and 0.9 V are not shown. The intensities are summarized in Figure 2. (c) Plots of the peak frequency for the 2-fold bridge CO band (2004−2029 cm^{-1}) vs the electrode potential in CO-saturated (blue curve) and in Ar-purged (red curve) solutions. Data obtained from Figure 1a.

of the electrode potential for CO-saturated (blue curve) and Ar-saturated (red curve) solution are summarized in Figure 2. Clearly, in the case of CO "stripping" experiments, the $I_{CO_2}-E$ and $I_{CO}-E$ plots show that the decrease in the CO_{ad} intensity at 0.7 V is mirrored by an increase in CO_2 production, indicating that CO is oxidatively removed from the surface. On the other hand, the onset of CO_2 production in the CO-saturated solution is not accompanied by a simultaneous decrease in the I_{CO} intensity, consistent with a continuous repopulation of unoccupied Au sites by dissolved CO. In the latter case, a significant decrease in the I_{CO} intensity is observed at 0.8 V, just before the disappearance of the CO stretching band in Figure 1a.

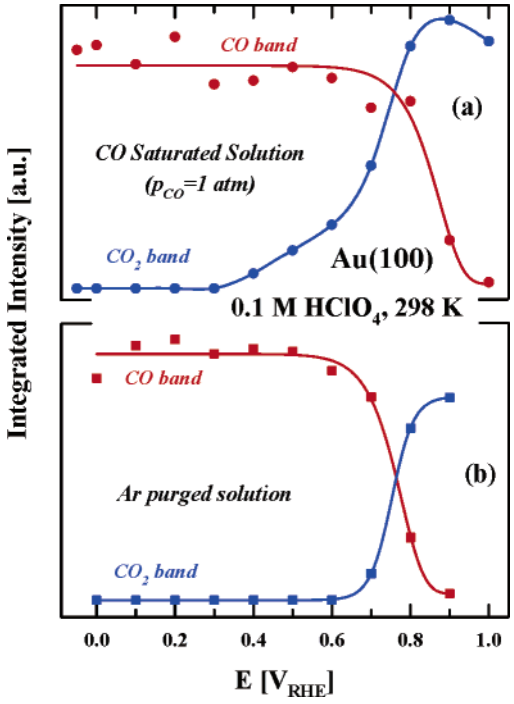

Figure 2. Integrated intensities of the CO and CO_2 bands as a function of the electrode potential. Data obtained from Figure 1a and b.

3.1.2. Au(111)-(1 × 23). Corresponding potential-dependent CO adsorption spectra on Au(111)-(1 × 23) in Ar-purged (red curves) and CO-saturated (blue curves) solution are shown in Figure 3a. Two CO stretching bands are obtained in CO-saturated solution; a major band (fwhm = 31 cm^{-1}) in the range 2029−2070 cm^{-1} and a relatively weak, yet readily discernible, C−O stretch (fwhm = 38 cm^{-1}) in the range 1946−1990 cm^{-1}. The insert in Figure 3 shows that in the presence of CO both band positions shift linearly with increasing the potential in the positive direction, at a rate of 50 cm^{-1} V^{-1} and 54 cm^{-1} V^{-1} for the high-frequency and the low-frequency CO band, respectively. Figure 3a also shows that purging with argon in order to remove CO from the solution yields the same high-frequency CO band as before, whereas the low-frequency CO band disappears entirely. Although the intensity of the CO band is different, slightly attenuated in the Ar-purged solution, the Stark tuning slope ($d\nu/dE$) is the same as that in the experiment with CO-saturated solution (i.e., in the insert of Figure 3, ∼50 cm^{-1} V^{-1}). Displayed in Figure 3b are the corresponding CO_2 stretching bands, which are used to establish the onset of CO oxidation on the Au(111)-(1 × 23) surface. Clearly, in CO−saturated solution the oxidative removal of CO (CO_2 production) starts at ∼0.5 V, which is significantly lower than the potential of 0.8 V observed in the "stripping" experiment. Plots of I_{CO} and I_{CO_2} as a function of the electrode potential in CO-saturated (blue curve) and in Ar-saturated (red curve) solutions are summarized in Figure 4. In contrast to the results of Figure 2, the $I_{CO_2}-E$ and $I_{CO}-E$ plots show that, irrespective of the experimental conditions, the decrease in the CO intensity at 0.5 V (in the presence of CO, Figure 4a) and at 0.8 V (in CO-free solution, Figure 4b) is mirrored by an increase in CO_2 production; i.e., in CO saturated solution, no or only little CO readsorption occurs. These results indicate that the adsorption of CO on the Au(111)-(1 × 23) surface is relatively weak

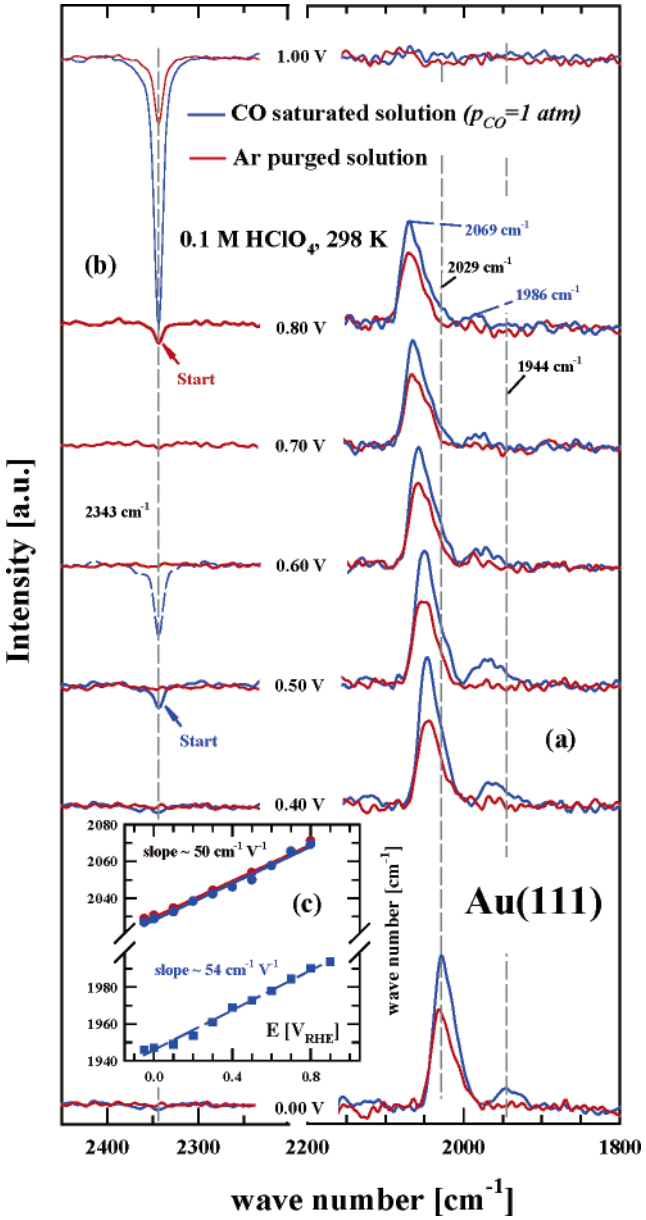

Figure 3. Same condition as those for Figure 1 but for the Au(111)-(1 × 23) surface. A major band in the 2029−2070 cm^{-1} range is attributed to 2-fold bridging CO; a weaker C−O stretch in the 1946−1990 cm^{-1} range is attributed to 3-fold bridging CO.

compared to the Au(100)-"hex" surface or, as will be shown below, to the Au(110)-(1 × 2) surface.

3.1.3. Au(110)-(1 × 2). In contrast to the other two Au low-index faces, infrared spectra of Au(110)-(1 × 2) in CO-saturated solution exhibit CO bands indicative of the presence of three distinct coordination geometries. As shown in Figure 5a, a CO stretching feature in the range of 1963−1994 cm^{-1} (fwhm = 31 cm^{-1}) dominates the spectra. A weaker CO band in the range of 2010−2030 cm^{-1} can also be seen under these conditions, and finally, an additional weak feature is discernible around 2115−2130 cm^{-1} (fwhm = 31 cm^{-1}). Corresponding Stark tuning plots of these three CO stretching bands are given in the insert of Figure 5. The highest slope is observed for the most intense band (~46 cm^{-1} V^{-1}); the high-frequency CO band position shifts linearly with a slope of 30 cm^{-1} V^{-1}. Markedly different behavior is observed in CO-free solution; illustrative potential-dependent spectra for the "stripping" conditions are

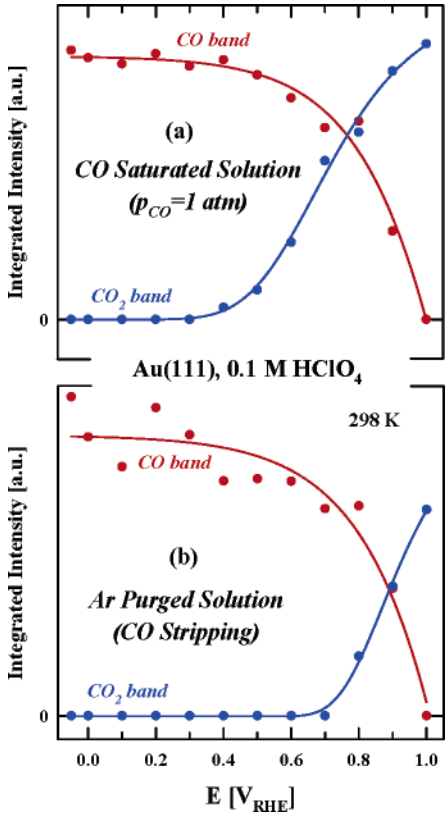

Figure 4. Integrated intensities of the CO and CO_2 bands as a function of electrode potential. Data obtained from Figure 3a and b.

shown in Figure 5a. Prominent are (i) the absence of the CO band in the 2115−2130 cm^{-1} range and (ii) the CO band at 2010−2030 cm^{-1} is much weaker (although clearly discernible) under these conditions, and (iii) the intensities for the CO band in the range of 1963−1994 cm^{-1} are attenuated in the absence of CO dissolved in the solution. As for the other two surfaces, oxidative removal of CO from the Au(110)-(1 × 2) surface was monitored by following the appearance of the CO_2 stretching band at 2343 cm^{-1}. Figure 5b reveals that, in CO-saturated solution, CO oxidation starts at as low as 0.4 V, which is again significantly lower than the value of 0.6 V observed in the "stripping" experiment. It is obvious, therefore, that, on all three Au single-crystal surfaces, CO oxidation has a positive reaction order with respect to the CO partial pressure. Plots of I_{CO} and I_{CO_2} as a function of electrode potential in the CO-saturated and Ar-saturated solutions are summarized in Figure 6a and b, respectively. Displayed in Figure 6a are plots of I_{CO_2}−E vs I_{CO}−E, the latter values being assessed by integrating the CO stretching bands around the 1963−1994 cm^{-1} (labeled as $I_{CO_{P1}}$), 2010−2030 cm^{-1} (labeled as $I_{CO_{P2}}$), and 2115−2130 cm^{-1} (labeled as $I_{CO_{P3}}$) range. Close inspection of Figure 6a reveals that initially (between −0.05 to 0.4 V) a decrease in the $I_{CO_{P2}}$ intensity is accompanied with an increase in $I_{CO_{P3}}$ and a monotonic increase in the I_{CO_2} intensity, suggesting that the initial CO electrooxidation is associated with an rearrangement of the CO adlayer. At more positive potentials, however, the increase in CO_2 production between 0.4 and 0.7 V parallels a fast decrease of $I_{CO_{P3}}$ and $I_{CO_{P2}}$, indicating that in this potential region the remaining CO adlayer has a tendency to occupy atop surface sites. In contrast, $I_{CO_{P1}}$ is constant up to 0.65 V, i.e., even in the potential region where CO oxidation occurs, and

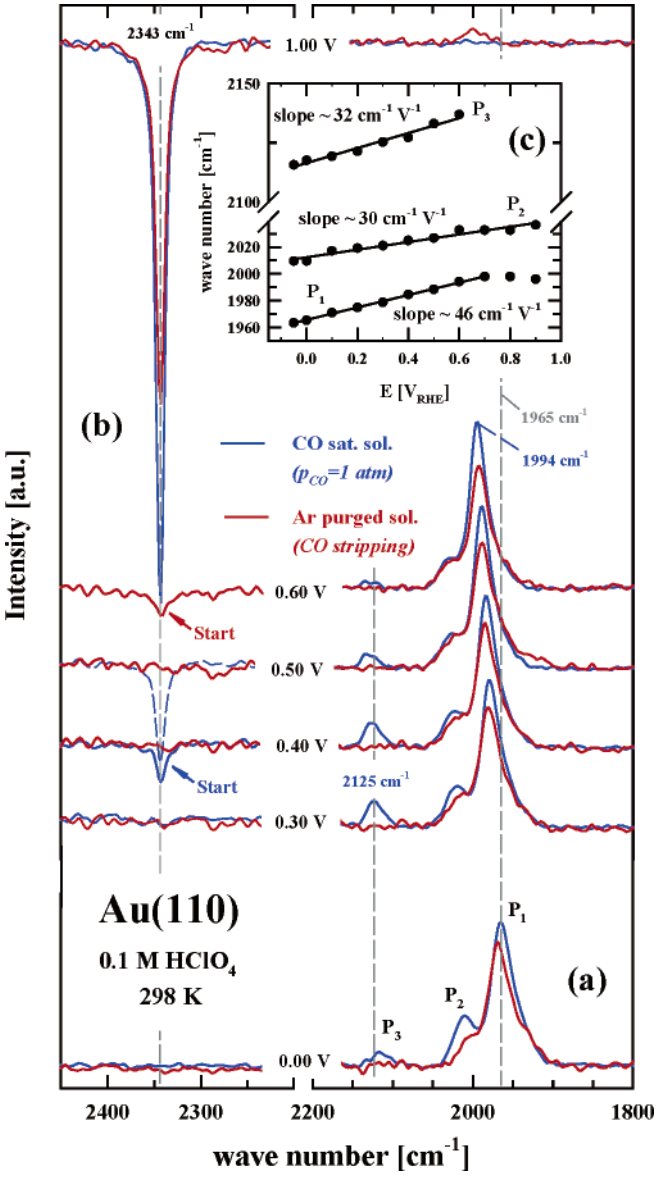

Figure 5. Same conditions as those for Figure 1 but for the Au(110)-(1 × 2) surface. The observation of three distinct C−O stretching vibrations is indicative for the presence of three distinct binding geometries: i.e., a weak terminal ν_{CO} feature at 2115 cm^{-1}, a stronger ν_{CO} band at 2010 cm^{-1}, attributed to 2-fold bridging, and a very strong ν_{CO} feature with low frequencies that may be consistent with a 3-fold bridging CO coordination geometry. Note, for clarity, the spectra between 0.6 and 0.9 V are not shown.

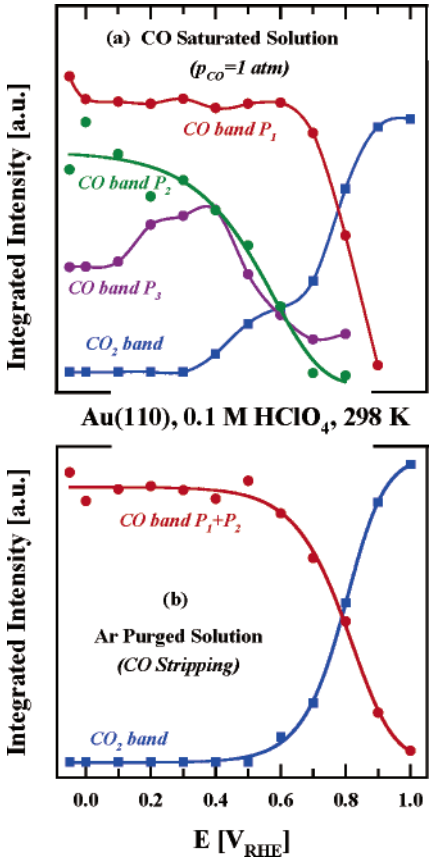

Figure 6. Integrated intensities of the CO and CO_2 bands as a function of electrode potential. Data obtained from Figure 5a and b.

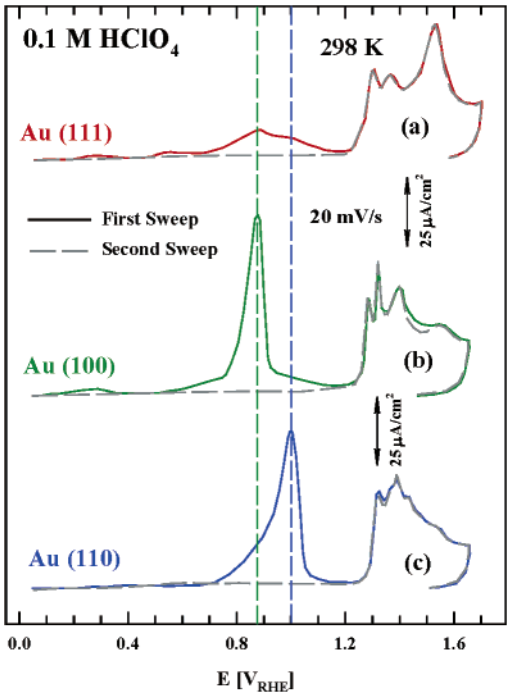

Figure 7. CO "stripping curves" in 0.1 M $HClO_4$: (a) Au(111)-(1 × 23), (b) Au(100)-"hex" and (c) Au(110)-(1 × 2). Sweep rate 20 mV/s. For details see text.

only at higher potentials the band intensity decreases rapidly. The results depicted in Figure 6a, therefore, clearly show that within $-0.05 < E < 0.65$ V, both the reactivity of the CO adlayer and the repopulation of the (110)-(1 × 2) surface by CO are site specific. In line with the other two single-crystal surfaces, for the Ar-purged solution $I_{CO_2}-E$ and $I_{CO}-E$ plots displayed in Figure 6b show the expected behavior; i.e., the decrease in the CO intensity at 0.8 V is accompanied by an increase in CO_2 production.

3.2. Electrochemical Measurements. 3.2.1. Stripping Curves of CO. Recall that in the CO "stripping" experiments prior to recording the oxidation currents, CO was completely removed from the solution by continuously purging the electrolyte with argon. The base voltammograms (only anodic parts) of the three low-index surfaces of Au in 0.1 M $HClO_4$, onto which is superimposed the anodic stripping voltammetry of CO, are shown in Figure 7.

In these experiments the positive potential limit was chosen so as to ensure that all preadsorbed CO was oxidized from the

surface. The fact that the successive negative-going sweep (not shown) and the second cycle (dashed gray curves in Figure 7) trace accurately the base voltammetry of the clean Au surface is the best confirmation that CO is completely "stripped" from the surface before the onset of irreversible oxide formation. Notice, at $E > 1.2$ V, all three single-crystal surfaces are unreconstructed, so the observed voltammetric features in this potential region correspond to the oxide formation on the (1 × 1) phase.[23] Upon sweeping the potential positively from −0.05 V, the onset of CO oxidation on Au(111)-(1 × 23) (red curve in Figure 7a) commences at ∼0.7 V, forming a rather broad peak with two small shoulders at 0.9 and 1.0 V. In the case of the Au(100)-"hex" surface, the onset of CO oxidation is observed at ∼0.65 V, producing first the preignition wave in the potential range 0.65−0.8 V and, then, a sharp peak centered at about 0.9 V. The shape of the CO stripping curve on Au(110)-(1 × 2) is rather similar; i.e., a small preoxidation wave starts to develop at ca. 0.75 V, which is followed by a sharp peak at 1.0 V. As will be seen in the next section, based on the position of the stripping peaks, one can misleadingly conclude that the least active surface for CO oxidation is Au(110)-(1 × 2). The integrated charge, assessed from the COad stripping peaks in Figure 7, corresponds to 145 ± 10% μC cm^{-2}, 350 ± 10% μC cm^{-2}, and 340 ± 10% μC cm^{-2} for Au(111)-(1 × 23), Au(100)-"hex", and Au(110)-(1 × 2), respectively. As discussed previously in the literature,[24] a reliable determination of the saturation coverage of CO by coulometric analysis of anodic stripping curves is far from straightforward and should be corrected from the contribution of the charge from the specific adsorption of anions, adsorption of hydroxyl species, and the double layer. Empirically, all three contributions can be approximated from the pseudocapacitance produced in the cyclic voltammetry in solution free of CO.[16] This charge should then be subtracted from the total charge assessed under the CO-stripping peak. Following this methodology, the fractional surface coverage of CO are ∼0.3, 0.72, and 0.95 ± 0.1 ML for Au(111)-(1 × 23), Au(100)-"hex", and Au(110)-(1 × 2) surfaces, respectively. For a CO adlayer, 1 ML is defined as one CO molecule adsorbed per Au surface atom of the reconstructed surfaces, i.e., 1.38 × 10^{15} atoms/cm^2, 1.19 × 10^{15} atoms/cm^2, and 0.84 × 10^{15} atoms/cm^2 for the Au(111)-(1 × 23) Au(100)-"hex", and Au(110)−(1 × 2) surface, respectively. We note that these coverages are much higher than the fractional coverage (ca. 0.1 ML) extracted from the quantity of CO_2 produced upon CO electrooxidation on Au(210) in the previous studies.[13,14]

3.2.2. Bulk oxidation of CO. Although the stripping voltammetry of CO_{ad} provides a valuable information about the kinetics of oxidation of adsorbed CO, only measurements with the continuous supply of CO to the electrode surface, such as with the RDE,[25] enables one to determine the true catalytic activity for the continuous oxidation of dissolved CO.

Current−potential curves for oxidation of dissolved CO on Au(111)-(1 × 23) (Figure 8a), Au(100)-"hex" (Figure 8b), and Au(110)-(1 × 2) (Figure 8c) all show a typical "bell-like" shape, i.e., a narrow (200 mV) region of mixed kinetic-diffusion control, which is followed by a diffusion-limiting plateau and then by rapid deactivation. Although it appears from the data in Figure 8 that the CO-oxidation reaction is structure insensitive, a comparison of the potential for the onset of CO oxidation on a magnified current scale (Figure 8) unambiguously shows that the rate of CO oxidation varies with crystal face; i.e., the activity increases in the order Au(110)-(1 × 2) ≥ Au(100)-"hex" > Au(111)-(1 × 23), in agreement with the onset of CO_2 production shown in Figures 1b, 3b, and 5b. The insert in Figure 8 shows Levich plots of i^{-1} versus $\omega^{-0.5}$ at 1.2 V, with a slope of $Bc_0 \approx 5.7 \times 10^{-2}$ mA/cm^2/rpm$^{0.5}$. The near zero intercept of the linear regression line in the Levich plots indicates that the current densities at the current plateaus are truly diffusion-limited. The experimental value of the Levich slope, obtained from Figure 8, is in excellent agreement with the theoretical value of $Bc_0 \approx 5.44 \times 10^{-2}$ mA/cm^2/rpm$^{0.5}$, based on the solubility of CO ($c_0 = 0.96 \times 10^{-3}$ M) and its diffusivity $D = 1.8 \times 10^{-5}$ cm^2/s for a two-electron oxidation process. Above 1.4 V, the currents are attenuated due to significant formation of an irreversible form (not reactive) of gold oxide.

4. Discussion

As already mentioned, the interpretation of previous EC/IRAS results was limited by several factors, including possible complications wrought by surface reconstruction of low-index Au single-crystal surfaces, a weak CO band intensity on Au (in particular, earlier studies showed no detectable ν_{CO} band on Au(100) and Au(111) surfaces[14]), and the lack of controlled transport of dissolved CO from the bulk of the solution to the electrode surface, a problem which is inherent to stationary electrodes used in all previous measurements. The present EC/IRAS results attempt to overcome some of these limitations and, hopefully, illustrate it is indeed possible to find a link between the macroscopic kinetic rate of the CO electrooxidation reaction and the coordination chemistry of CO adsorbed on Au single-crystal surfaces.

4.1. Surface Reconstruction at the Au(*hkl*)−CO Interface. The phenomenon of surface reconstruction has been described at some length in reviews published quite recently,[1,23,26,27] and accordingly the discussion here will concentrate only on those principles and effects, which are of direct relevance for the results presented in the previous section. As shown in Figure 9, the structures of reconstructed Au surfaces are very different from each other, a consequence of the very different bulk termination. Recent studies using the in situ SXS technique provided very important information regarding the potential-dependent structure stability of the "reconstructed" ↔ (1 × 1) transition (hereafter denoted as the "rec" → (1 × 1) transition) of Au single crystals in an electrochemical environment.[23,28,29] These measurements have revealed that at −0.05 V all three low-index single-crystal surfaces of Au are reconstructed. The most dramatic change during reconstruction occurs on the (100) face: the reconstruction (formally called the "hex" phase) consists of a distorted hexagonal overlayer with a 24% higher atomic surface density than the underlying (1 × 1) square substrate (Figure 9). On the positive sweep from −0.05 V (2 mV s^{-}), no structure changes appear until 0.6 V, above which the "hex" reconstruction is gradually transformed to the (1 × 1) structure. The (111) reconstruction (known as the (1 × 23) phase) has a more subtle uniaxial compression (ca. 4%) of the

(23) Lucas, C. A.; Markovic, N. M. Encyclopedia of Electrochemistry. [2], sectuin 4.1.2.1.2. 2004. Wiley-VCH. Ref Type: Serial (Book, Monograph).
(24) Weaver, M. J.; Chang, S. C.; Leung, L. W. H.; Jiang, X.; Rubel, M.; Szklarczyk, M.; Zurawski, D.; Wieckowski, A. *J. Electroanal. Chem.* **1992**, *327*, 247−260.
(25) Albery, W. J.; Hitchman, M. L. *Ring-Disc Electrodes*; Clarendon Press: Oxford, 1971.

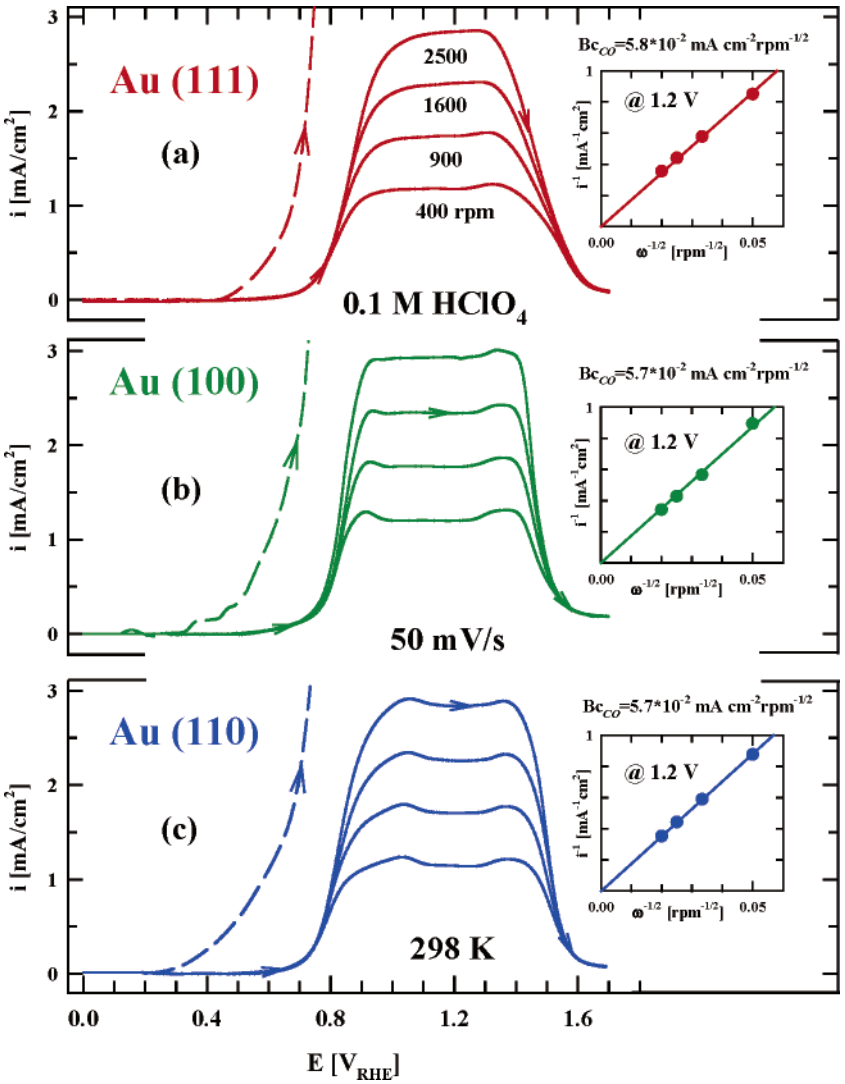

Figure 8. Polarization curves (20 mV/s) for the electrooxidation of bulk CO on (a) Au(111)-(1 × 23), (b) Au(100)-"hex", and (c) Au(110)-(1 × 2). Inserts: corresponding Levich plots.

top layer (see Figure 9). Starting at −0.05 V and sweeping the potential positively (2 mV s^{-}), the (1 × 23) reconstruction begins to "lift" at ∼0.7 V and continues to transform to the (1 × 1) phase up to ∼1.0 V. Although the "hex" and the (1 × 23) reconstructed surfaces have similar distorted hexagonal symmetries (Figure 9), the surface strain is different as is the characteristic domain size. As will be shown in the subsequent sections, such strained overlayers can have chemical properties that are significantly different from each other. Theoretically, the effect of strain on the reactivity of metal surfaces has recently been discussed by Mavrikakis et al..[30] As depicted in Figure 9, at −0.05 V the open (110) face reconstructs to form a (1 × 2) "missing row" structure which results in the formation of microscopic (111) facets. In some experiments a mixture of (1 × 2) and (1 × 3) structures was observed, the latter consisting of deeper grooves and larger (111) microfacets; i.e., while the (1 × 2) structure consists of two atom wide terraces in the (1 × 3) structure, monatomic steps with the (111) orientation are separated by three atom wide terraces. Above −0.05 V, the (1 × 2) structure is stable up to ∼0.5 V, above which a relatively slow (1 × 2) ↔ (1 × 1) transition is observed in SXS measurements. In agreement with respective investigations in ultrahigh vacuum (UHV) 23, in an electrochemical environment the reconstructed phase of the clean Au(*hkl*) surfaces can be "lifted" by adsorption of atoms or molecules.[1,23,26,27] In 0.1 M $HClO_4$, the electrolyte used in this work, the reconstruction of Au(111), Au(100), and Au(110) is lifted by the adsorption of oxygenated species and anions of the supporting electrolyte.[16]

Equally important, yet much less studied, is the effect of CO on the thermodynamics of the "rec" → (1 × 1) transition in an electrochemical environment. More recently, SXS studies in acid solution found that, in contrast to the effects of anionic adsorbates, CO has an effect neither on the potential range of the "rec" → (1 × 1) transition nor on the surface relaxation,[16] indicating that the Au(*hkl*)−anion interaction is much stronger than the Au(*hkl*)−CO interaction.

4.2. Assignment of Adsorption Sites at the Au(*hkl*) Interface. There were two significant new pieces of information provided by the IRAS results that help us to gain insight into the interaction of CO with reconstructed gold single-crystal surfaces.

(1) The first characteristic is that Au surfaces with different morphologies give rise to unique C−O band frequency positions, as summarized in Figure 9a. To interpret these results, we assume that each of the characteristic features in the CO spectra is associated with a specific binding site on the Au single-crystal

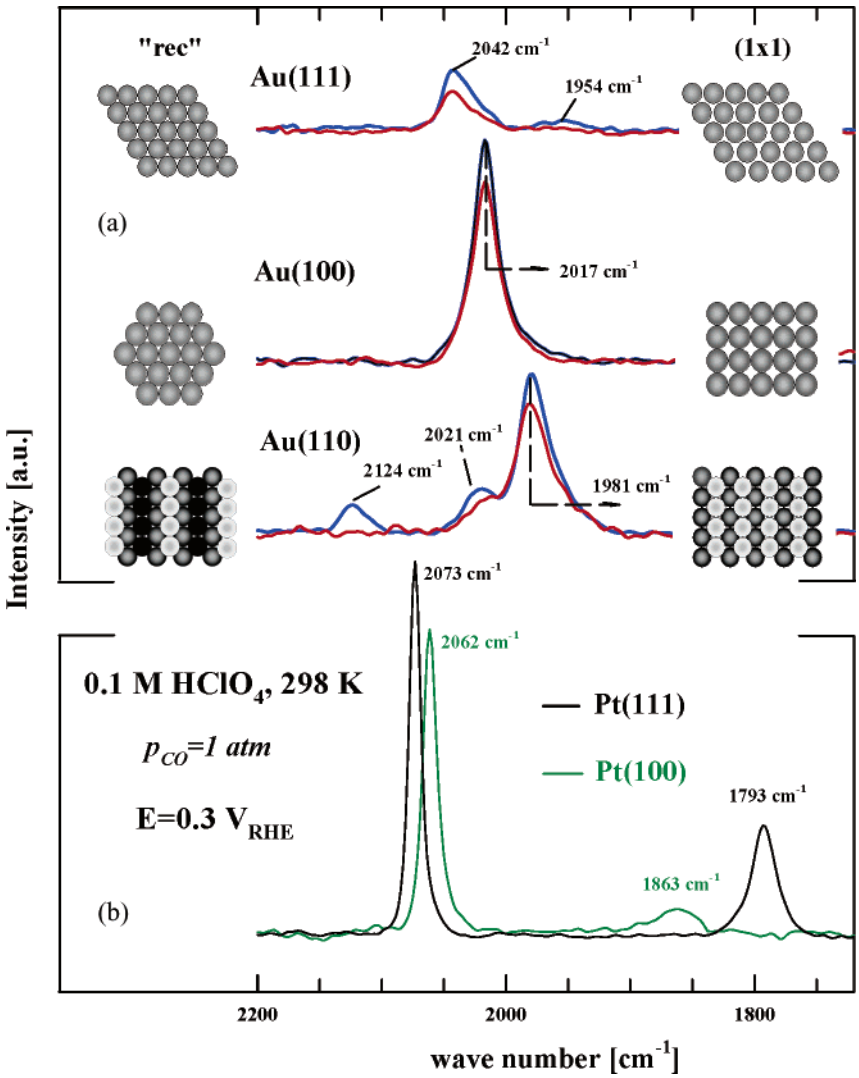

Figure 9. (a) Representative spectra for the C−O stretching frequency on Au(*hkl*) in 0.1 M $HClO_4$ saturated with CO (blue curves) and in Ar-purged solution (red curves). Notice, the C−O stretching frequency is sensitive to the geometry of the adsorption sites and can be observed in the range 1940−1990 cm^{-1} for the 3-fold bridging, 2005−2070 cm^{-1} for the 2-fold bridging, and 2115−2140 cm^{-1} for the terminal position. A simple schematic model of the Au(111)-(1 × 23), Au(100)-"hex", and Au(110)-(1 × 2) reconstructions and corresponding unreconstructed structures is shown. (b) Corresponding spectra for the CO band on Pt(100) and Pt(111) in 0.1 M $HClO_4$ saturated with CO. These two surfaces are used to emphasize that the terminal, 2-fold bridge, and 3-fold bridge CO bands are red shifted relative to the C−O frequencies on Au(*hkl*).

surfaces and assign these coordinations in analogy to the corresponding CO band frequencies/intensities on Pt single-crystal surfaces. The two representative spectra for CO adsorbed on Pt(100) and Pt(111), summarized in Figure 9b having the same intensity scale as that for Au(*hkl*), were used to make these assignments. Collected in Table 1 are both the relevant physicochemical properties for a CO adlayer on Au and Pt and the corresponding ν_{CO} frequencies on Au(*hkl*) and Pt(*hkl*) in CO-saturated solution.

In CO-saturated solution, the most complex spectra are observed on the "stepped" Au(110)-(1 × 2) surface covered with ∼1 ML of CO. The most intense feature (in Figure 5 at all potentials) of the spectrum is a band near 1965 cm^{-1}, with the second, weaker band shifted positively by about 45 cm^{-1} above it and, finally, a weak band near 2115 cm^{-1}. The presence of three distinct C−O stretching vibrations is indicative of the presence of three distinct binding geometries: i.e., a weak terminal ν_{CO} feature at 2115 cm^{-1} (i.e., coordination to a single gold atom), a stronger ν_{CO} band at 2010 cm^{-1}, attributed to 2-fold bridging (i.e., coordination to two gold atoms), and a very strong ν_{CO} feature at 1965 cm^{-1} that may be consistent with the 3-fold bridging (i.e., coordination to three gold atoms) coordination geometry. In an earlier investigation, the low-frequency and the high-frequency bands were also observed under similar experimental conditions (CO dosing time of ca. 10 min) on the stepped Au(210) surface, but no band at 2010 cm^{-1} was detected by Chang et al..[14] The authors attributed the high-frequency band at 2110 cm^{-1} to linearly bonded CO and the low-frequency band with a large ν_{CO} frequency−potential dependence to a bridging CO coordination geometry. In contrast to an electrochemical environment, a single C−O band is observed on Au(110)-(1 × 2) in UHV, depending on experimental conditions the CO band is centered in the range of 2118 to 2108 cm^{-1}.[31−33]

(26) Kolb, D. M. *Prog. Surf. Sci.* **1996**, *51*, 109−173.
(27) Magnussen, O. M. *Chem. Rev.* **2002**, *102*, 679−725.
(28) Ocko, B. M.; Wang, J.; Davenport, A.; Isaacs, H. *Phys. Rev. Lett.* **1990**, *65*, 1466−1469.
(29) Toney, M. F.; Ocko, B. M. *Synchrotron Radiat. News* **1993**, *6*, 28−33.
(30) Mavrikakis, M.; Hammer, B.; Norskov, J. K. *Phys. Rev. Lett.* **1998**, *81*, 2819−2822.
(31) Ruggiero, C.; Hollins, P. *Surf. Sci.* **1997**, *377−379*, 583−586.

Table 1. Summary of the Relevant Physicochemical Properties for a CO Adlayer on Au and Pt as Well as the Corresponding ν_{CO} Frequencies on Au(*hkl*) and Pt(*hkl*) in CO-Saturated Solution[a]

		Au(*hkl*)			Pt(*hkl*)		
"rec" → (1 × 1) transition			yes			no	
expansion [%]			0			∼4−25	
ΔG_{CO_g} [kJ/mol]			55 (0 ML) 35 (0.45 ML)			160 (0 ML) 55 (1 ML)	
Φ [eV]			−0.95			+1.0	
$\Theta_{CO_{ad}}$ [ML]		(111)	(100)	(110)	(111)	(100)	(110)
		0.3	0.72	0.95	0.75	0.82	1
ν [cm^{-1}] at 0.0 V	multi	1946		1963	1779	1886	
	bridge	2027	2004	2009	2065	2049	
	atop				2116		2072
$\partial\nu/\partial\Theta_{CO}$			positive			negative	
ordered structures			no			yes	
dipole shift			positive			positive	
chemical shift			negative			positive	
M → $2\pi^*$ donation			unimportant			important	
5σ → M donation			important			unimportant	
reaction order			positive			negative	

[a] ΔG_{CO_g}: energy of adsorption of CO in the gas phase. Φ: change in the work function upon CO adsorption in UHV. $\Theta_{CO_{ad}}$: CO saturation surface coverage obtained from Figure 7. $\partial\nu/\partial\Theta_{CO}$: Change in the C−O stretch frequency with CO surface coverage in UHV.

To the best of our knowledge, no vibrational spectra for CO adsorbed on Au(111) have been reported previously in either an electrochemical or UHV environment. The spectrum for the C−O stretching frequency on Au(111)-(1 × 23) depicted in Figure 9a is, therefore, the first result of its kind and is less complex than for CO adsorbed on Au(110)-(1 × 2). In particular, a weak ν_{CO} band at 2040 cm^{-1}, attributed to 2-fold bridging CO, dominates the spectra. An even weaker ν_{CO} band, which is red-shifted to 1954 cm^{-1}, is consistent with 3-fold bridging CO. Aside from our preliminary report for the C−O stretching band on Au(100)-"hex" in acid solution,[16] there are no other IRAS studies of the adsorption states and the interaction of CO with this surface. In agreement with ref 16, and in contrast to the other Au low-index faces, the IRAS spectra of CO adsorbed on the Au(100)-"hex" surface exhibit only a single band frequency at 2004−2029 cm^{-1}. The fact that we observe only one CO absorption band on Au(100)-"hex" allows the unambiguous assignment of the frequency in Figure 9a at 2017 cm^{-1} to a 2-fold bridging CO. Recall that even though the "hex" and the (1 × 23) surface have a very similar arrangement of surface atoms, the chemical properties of these two surfaces are significantly different from each other, reflecting the importance of strain for the adsorption properties on metal surfaces.[30]

Similarly to Pt(*hkl*),[34] the sensitivity of the C−O vibrational frequency to the adsorption geometry is also observed on Au single crystals. Figure 9b shows, however, that the C−O frequency band on Pt(100) and Pt(111) gives rise to a substantially lower C−O frequency under similar experimental conditions. For example, at 0.0 V the difference in ν_{CO} on Au and Pt (data for ν_{CO} are contained in Table 1) lies in the range of about 50 cm^{-1}, 200 cm^{-1}, and 150 cm^{-1} for the terminal, 2-fold bridging, and 3-fold bridging coordination geometry, respectively. The observed differences can be explained by a much weaker Au−CO interaction than the Pt−CO interaction. A weak interaction of CO with Au is well documented in the gas phase; i.e., UHV data analysis revealed that the isosteric heat of CO adsorption on Au varies from ∼58 kJ/mol (Θ_{CO} → 0 ML) to 35 kJ/mol (Θ_{CO} → 0.45 ML),[33,35−37] which is significantly lower than 160 kJ/mol (Θ_{CO} → 0 ML) and 55 kJ/mol (Θ_{CO} → 0.75 ML) found for Pt under similar experimental conditions[1] (see Table 1). Comparison between the change in the work function upon the adsorption of CO on Au and Pt (inferred from UHV measurements) are also listed in Table 1. Significantly, while the work function of Au(110)-(1 × 2) *decreases* (∼ −0.95 eV) upon CO adsorption, the work function on transition metals *increases* (+1 eV or more)[37] upon CO adsorption. As we discuss below, the observed difference in the change of the work function upon the adsorption of CO on Au and Pt may explain the difference in the chemical shifts induced by changes in the CO coverage on these two metals.

In "argon-purged" solution, significantly different infrared spectra were obtained than in CO-saturated solution, which is also in agreement with the interaction of CO with Pt(111).[38] Most notably, as shown in Figure 9a, under conditions without continuous repopulation of the surface with CO, the terminal ν_{co} band on Au(110)-(1 × 2) and the 3-fold bridging band on Au(111)-(1 × 23) disappear entirely. In the case of Au(100)-"hex", in Ar-purged solution the integrated intensities of the peak at 2004−2029 cm^{-1} are attenuated with respect to the experiments in CO-saturated solution. The fact that the formation of a saturated CO adlayer requires a continuous overpressure of CO even at such low potentials (−0.05 V) is a further indication of the weak Au−CO interaction. The question arises, however, whether the decrease in the surface coverage by CO in Ar-saturated solution is a consequence of kinetic or thermodynamic effects; i.e., it is unclear if, without continuous repopulation of the adsorption sites by bulk CO, the change in CO coverage is caused by electrooxidation of irreversibly adsorbed CO and/or by reversible desorption of CO_{ad}. The amount of adsorbed CO depends on the pressure of CO gas. For the time being, it is experimentally impossible to confirm unambiguously which process is the predominant one.

(32) Jugnet, Y.; Cadete Santos Aires, F. J.; Deranlot, C.; Piccolo, L.; Bertolini, J. C. *Surf. Sci. Lett.* **2002**, *521*, L639-L644.
(33) Meier, D. C.; Bukhtiyarov, V.; Goodman, D. W. *J. Phys. Chem. B* **2003**, *107*, 12668−12671.
(34) Chang, S. C.; Weaver, M. J. *Surf. Sci.* **1990**, *238*, 142−162.
(35) Kottke, M. L.; Greenler, G. R.; Tompkins, H. G. *Surf. Sci.* **1972**, *32*, 231−243.
(36) McElhiney, G.; Pritchard, J. *Surf. Sci.* **1976**, *60*, 397−410.
(37) Gottfried, J. M.; Schmidt, K. J.; Schroeder, S. L. M.; Christmann, K. *Surf. Sci.* **2003**, *536*, 206−224.
(38) Villegas, I.; Weaver, M. J. *J. Chem. Phys.* **1994**, *101*, 1648.

Nevertheless, regardless of the main cause of the decrease in the surface coverage by CO under Ar-purged conditions, a close inspection of Figure 9a clearly indicates that, as the coverage increases the CO band shifts either slightly (2−4 cm^{-1}) to *lower* wavenumbers, as in the case of Au(111)-(1 × 23) and Au(110)-(1 × 2), or stays the same, as in the case of Au(100)-"hex". Interestingly, an opposite behavior has been observed for the Pt−CO system;[34] i.e., as the CO coverage increases, the CO band shifts significantly to *higher* wavenumbers. The difference between the two metals can be rationalized, at least qualitatively, in terms of two contributions: (i) the chemical interaction between CO and the substrate (the chemical shift) and (ii) the CO−CO lateral interactions (the dipole−dipole coupling shift).

A theoretical description of the chemical shift has been given with the back-bonding model of Blyholder;[39] i.e., the chemical bond between CO and metal is formed by charge transfer from the weakly (anti)bonding 5σ orbital of CO into the metal and by back-donation from metal into the strongly antibonding 2π* orbital. Notice that no consistent interpretation has been proposed for the nature of the 5σ orbital; while some suggested that the 5σ orbital is weakly antibonding,[31] others are considering the 5σ orbital to be weakly bonding.[40] For our discussion, we use the approach of Hollins and co-workers,[31,41] who have considered the 5σ molecular orbital to be weakly antibonding. According to these authors, the different balance between 5σ and 2π* bonding shown by Au and Pt is the major factor in determining the chemical shift. In particular, in contrast to the Pt−CO system, back-donation of electrons into the 2π* orbital of the CO molecule is relatively unimportant for Au (as well as for other elements from the Group IB metals) and the bonding is consequently dominated by the 5σ orbital, Table 1. As the CO coverage increases and bonding becomes energetically less favorable (see the value of ΔG in Table 1), it is likely that less donation from the 5σ orbital will occur, resulting in a weaker C−O bonding. This, in turn, will be reflected by a downshift in the C−O stretch frequency (a *negative* chemical shift). Transition metals such as Pt, which do exhibit a significant degree of back-donation into the 2π* orbital (which is why the change in work function upon adsorption of CO is exactly the opposite from Au), naturally demonstrate the opposite effect. At low CO coverage, when the energy of CO adsorption is in the range of ∼160 kJ/mol (Table 1), a substantial degree of back-donation into the 2π* orbital occurs, a fact which is consistent with a substantial weakening of the C−O bond at low Θ_{CO}. On the other hand, when the energy of adsorption is reduced at higher CO coverage (Table 1), the degree of back-donation into the 2π* is significantly reduced, resulting in a stronger C−O bond, with a consequent enhancement in vibrational frequency relative to low Θ_{CO}. As a result, by increasing Θ_{CO}, a *positive* chemical shift has been measured at Pt in UHV [41] as well as in an electrochemical environment.[34] In contrast to the chemical shift, the dipole coupling shift is independent of the nature of the substrate and always tends to increase the C−O frequency at higher CO coverage. In real systems, these two terms have a tendency either to compensate each other, i.e., the Au−CO system, or to superimpose on each other, i.e., the Pt−CO system.

In adopting the UHV approach, it is reasonable to suggest that the coverage dependence of the CO adsorption spectra on Au single-crystal surfaces in acid solution is a consequence of two opposing effects: a dipolar coupling shift which tends to increase the frequency at a higher coverage and a chemical shift which tends to reduce it. Clearly, the balance between these two opposing effects varies slightly from one Au crystal face to another, so that the net shift may be either slightly negative, as for Au(111)-(1 × 23) and Au(110)-(1 × 2), or zero, i.e., both effects cancel each other, as for Au(100)-"hex". Various details of CO interaction with Au in an electrochemical environment are, however, still unresolved, and many effects, including the presence of coadsorbed solvents and the variation of the electrode potential (hence surface potential), should be included in the analysis in order to resolve the vibrational properties of the Au−CO system. The present emergence and rapid ongoing development of computational methods[42,43] may help and even transform our understanding of vibrational spectra of CO adsorption on Au single-crystal surfaces.

(2) The second characteristic is that both the intensities as well as the shape of the CO spectra on Au single crystals are strongly dependent on the surface orientation, as summarized in Figure 9. The fact that the CO band on Au(111)-(1 × 23) is much weaker than that on the other two single-crystal surfaces is consistent with the low CO saturation coverage (in Table 1, ca. 0.3 ML). As a consequence, rather broad ν_{CO} bands are observed on the Au(111)-(1 × 23) surface. The low-frequency absorption tail of the CO band on Au(111)-(1 × 23) may be characteristic of a vibrational coupling between randomly distributed molecules in small islands with repulsive intermolecular forces. On the other hand, on the highly corrugated (strained) Au(100)-"hex" and "stepped" Au(110)-(1 × 2) surfaces, the surface−CO interaction is much stronger, resulting in a higher CO saturation coverage on both surfaces (see Table 1). Consequently, relative sharp C−O bands are observed on the Au(110)-(1 × 2) surface and especially on the Au(100)-"hex" surface. It is worth noting that even though a sharp C−O band on Au(100)-"hex" may indicate some degree of ordering of the CO adlayer, no ordered CO structure was observed in our SXS experiments on this surface.[16] Interestingly, and in contrast to previous findings,[14,44] the integrated intensities of both the 2-fold bridging C−O band on (100)-"hex" and the 3-fold bridging C−O band on (110)-(1 × 2) are comparable to the band intensities of CO adsorbed on Pt(100)-(1 × 1) and Pt(111)-(1 × 1). This finding is new and at variance with previous suggestions that the maximum surface coverage of CO on Au is very low (ca. 0.1 ML) in comparison with Pt.[14]

4.3. Structure Sensitivity and Reaction Mechanism. A great deal of work in surface electrochemistry has been aimed at elucidating the role of the local symmetry of surface atoms for the rate of a reaction,[1,6,23] generally termed as structure sensitivity. For example, it has been found that the structure sensitivity of CO oxidation on Pt single-crystal surfaces mainly arises due to the structure sensitive adsorption of CO, oxygen-containing species, and spectator species such as anions from the supporting electrolyte. Just as for the Pt(*hkl*)−CO systems,

(39) Blyholder, G. *J. Phys. Chem.* **1964**, *68*, 2772.
(40) Hoffman, F. *Surf. Sci. Rep.* **1983**, *3*, 107−192.
(41) Hollins, P. *Surf. Sci. Rep.* **1992**, *16*, 51−94.
(42) Hammer B.; Norskov, J. K. *Chemisorption and Reactivity on Supported Clusters and Thin Films*; Kluwer Academic Publisher: 1997; pp 285−351.
(43) Hammer, B.; Norskov, J. K. *Adv. Catal.* **2000**, *45*, 71.
(44) Kim, C. S.; Korzeniewski, C.; Tornquist, W. J. *J. Chem. Phys.* **1993**, *100*, 628−630.

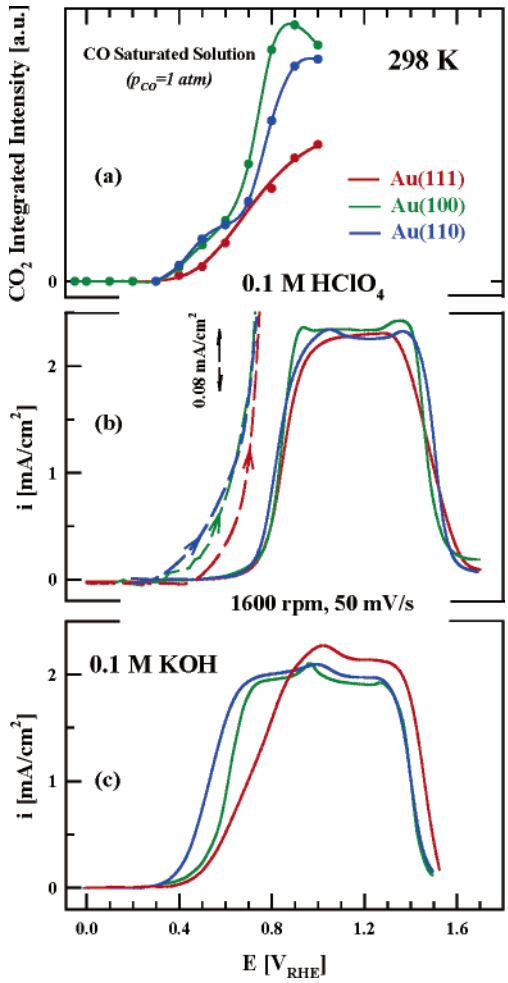

Figure 10. Structure sensitivity of Au(*hkl*) established by comparing the following: (a) CO_2 production in 0.1 M $HClO_4$, saturated with CO; (b) the polarization curves in 0.1 M $HClO_4$ saturated with CO (solid curves); to emphasize the onset of CO oxidation, the CO currents at low potentials (dashed curves) are magnified by a factor of 5; (c) the polarization curves in 0.1 M KOH saturated with CO.

the difference in activity of the three low-index surfaces of Au for CO oxidation, which is presented in section 3, will in the following be discussed in the light of the structure sensitive adsorption of reacting and spectator species.

As revealed in Figure 10, the rate of CO oxidation varies with the crystal face, i.e., Au(110)-(1 × 2) and Au(100)-"hex" being more active than Au(111)-(1 × 23). Interestingly, the same order of activity is observed by using either IRAS measurements shown in Figure 10a or RDE measurements shown in Figure 10b, indicating that the catalytic activity of Au single-crystal surfaces can independently be followed by monitoring the development of the O−C−O stretching band or by measuring polarization curves. Furthermore, the results in section 3.1 have revealed that, in the potential region where the Au(*hkl*) surfaces are reconstructed ($\sim -0.05 < E < 0.7$ V), both the reactivity of the CO adlayer and the repopulation of the surface by CO during the electrooxidation reaction are site-specific. For example, Figure 6a reveals that initially a decrease in the $I_{CO_{P2}}$ intensity is accompanied with an increase in $I_{CO_{P3}}$ and a monotonic increase in the I_{CO_2} intensity, suggesting that the initial CO electrooxidation is accompanied by a rearrangement of the CO adlayer. The fact that on Au(110)-(1 × 2) the bridging and multicoordinating sites have disappeared first does not necessarily imply that on these sites preferential oxidation of CO takes place. Rather, during CO electrooxidation (the active sites are most likely the step-trough combination, i.e., CO on the (111) facets and OH on the top rows of surface atoms, in analogy with ref 45 for the Pt−CO system) on Au(110)-(1 × 2), the remaining CO adlayer will rearrange most plausibly to yield lower Θ_{CO} values in order to diminish CO−CO repulsion and to optimize the CO binding-site energetics. The proposed alteration of the CO adsorption sites in the course of the reaction is in agreement with a dipole-coupling analysis of coverage-dependent CO infrared spectra on transition metal surfaces.[46,47]

On all three surfaces, the appearance of CO_2 is mirrored by the concomitant decrease in the CO band intensities (see Figures 1, 3, and 5) and with the onset of adsorption of hydroxyl species on a polycrystalline Au electrode in 0.1 M $HClO_4$,[48,49] consistent with the Langmuir−Hinshelwood (L−H) reaction mechanism, i.e.,

$$CO_{ad} + OH_{ad} = CO_2 + H^+ + e^- \quad (1)$$

In the framework of the above discussion, the general rate expression for the reaction 1 can be given by

$$i = nFk(1 - \Theta_{CO_{ad}} - Q_{OH_{ad}} - \Theta_{ClO_{4(ad)}^-;Cl_{ad}}) \exp(-\beta FE/RT) \exp(-r\Theta_{ad}/RT) \quad (2)$$

where i is the observed current density, n is the number of electrons, k is the rate constant, Θ_{ad} is the total surface coverage by adsorbed CO_{ad} ($\Theta_{CO_{ad}}$), OH_{ad} ($\Theta_{OH_{ad}}$), and $ClO_{4_{(ad)}}^-/Cl_{ad}$ anions ($\Theta_{ClO_{4(ad)}^-;Cl_{ad}}$) (in perchloric acid solution, specifically adsorbing anions have been proposed to be either ClO_4^-[49,50] and/or Cl^-,[51,52] the latter being present as an impurity even in the most meticulously prepared electrolyte), β is the symmetry factor, E is the applied potential, and $r\Theta_{ad}$ is an energetic parameter characterizing the rate of change of the apparent standard free energy of activation with the surface coverage of adsorbed species. Theoretically, for weakly adsorbed CO (≤30 kJ/mol), a maximum reaction rate of 1 would require the Au surface to be free of specifically adsorbed anions ($\Theta_{ClO_{4(ad)}^-;Cl_{ad}} = 0$ ML) and half covered with the respective electroactive species ($\Theta_{CO_{ad}} = \Theta_{OH_{ad}} = 0.5$ ML). Experimentally, we can see this balance in action by examining the structure sensitivity of CO oxidation reaction first in acidic and then in alkaline media. The discussion will be focused on the onset of the CO oxidation reaction, i.e., in the potential region where *reversibly* adsorbed OH_{ad} and $ClO_{4_{ad}}^-/Cl_{ad}$ compete for the Au surface covered with a saturated layer of *irreversibly* adsorbed CO. In the following, the objective is to determine where, at least qualitatively, we might expect to see the surface geometry play a major role.

Interestingly, the Au(110)-(1 × 2) and Au(100)-"hex" surfaces, which are covered with almost a full CO monolayer,

(45) Lebedeva, N. P.; Rodes, A.; Feliu, J. M.; Koper, M. T. M.; van Santen, R. A. *J. Phys. Chem. B* **2002**, *106*, 9863−9872.
(46) Severson, M. W.; Stuhlmann, C.; Villegas, I.; Weaver, M. J. *J. Chem. Phys.* **1995**, *103*, 9832−9843.
(47) Severson, M. W.; Weaver, M. J. *Langmuir* **2005**, 5603−5611.
(48) Zou, S.; Zemlyanov, E. R.; Weaver, M. J. *Langmuir* **2000**, *16*, 754−763.
(49) Li, X.; Gewirth, A. A. *J. Am. Chem. Soc.* **2003**, *125*, 7080−7099.
(50) Ataka, K.; Yotsuyanagi, T.; Osawa, M. *J. Phys. Chem.* **2003**, *100*, 10664−10672.
(51) Markovic, N. M.; Hanson, M.; McDougal, G.; Yeager, E. *J. Electroanal. Chem.* **1986**, *241*, 309.
(52) Markovic, N. M.; Ross, P. N. *J. Electroanal. Chem.* **1992**, *330*, 499−520.

are more active for CO oxidation than the Au(111)−(1 × 23) surface, which is covered only partially with CO ($\Theta_{CO_{ad}} \approx 0.3$ ML). Three hypotheses can be invoked in order to explain this structure sensitivity: (i) CO is weakly adsorbed on Au and thus at a certain potential, i.e., surface charge, can be displaced from surface sites by OH_{ad} and $ClO_{4_{ad}}^-/Cl_{ad}$; (ii) preferential displacement by OH_{ad} and $ClO_{4_{ad}}^-/Cl_{ad}$ occurs at or above the potential of zero charge at low-coordination Au atoms (the "active site model" [42,53]); and (iii) if an ensemble of CO-free Au sites is large enough on an otherwise CO-covered surface, $ClO_{4_{ad}}^-/Cl_{ad}$ will block the adsorption of OH_{ad} on these sites. Our supposition that CO can be displaced from certain Au surface sites by OH_{ad} and $ClO_{4_{ad}}^-/Cl_{ad}$ is based on the fact that below $E < 0.6$ V the interaction strength increases in the order Au(*hkl*)−CO ≪ Au(*hkl*)−OH_{ad} < Au(*hkl*)−$ClO_{4_{ad}}^-/Cl_{ad}$; for details, see ref 16. Notice that the fractional surface coverage by OH_{ad} and $ClO_{4_{ad}}^-/Cl_{ad}$ will depend on the adsorption isotherm, which relates the surface concentration to the bulk concentration and, more importantly, to the potential of zero charge. At $E < 0.6$, a rather small (<0.1 ML) fractional coverage of OH_{ad} and $ClO_{4_{ad}}^-/Cl_{ad}$ can be inferred from the cyclic voltammetry of Au(*hkl*) surfaces in 0.1 M $HClO_4$. This, in turn, may explain why the saturated coverage of irreversibly adsorbed CO stays intact in a wide potential range. The effect of active sites can be understood if we consider an observation made previously[1] and restated here that the initial adsorption of OH occurs at low-coordination sites at the Au(*hkl*)−CO surface. Given that the (1 × 2) surface is fully stepped and that the Au(111)-(1 × 23) surface is the least stepped/strained surface, it is reasonable to propose that the fractional surface coverage by OH_{ad} should increase in the order (1 × 23) < "hex" < (1 × 2). Translated into eq 2, this would imply that in the absence of specifically adsorbing anions the least active for the electrooxidation of CO should be the Au(111)-(1 × 23) surface and the most active should be the Au(110)-(1 × 2) surface. To test our concept, we chose to examine the electrooxidation of CO on all three Au single-crystal surfaces but in alkaline solution, i.e., in an environment where the surface coverage by OH_{ad} is only limited by the number of low-coordination sites and not by the competitive adsorption with $ClO_{4_{ad}}^-/Cl_{ad}$. The fact that the activity for CO oxidation in 0.1 M KOH increases in the same order, i.e., Au(111)-(1 × 23) < Au(100)-"hex"< Au(110)-(1 × 2), is the best confirmation that structure sensitivity arises mainly due the to structure sensitive number of low-coordinated atoms on the Au(*hkl*) surfaces. In acid solution, however, the rate of reaction 2 is attenuated because some active sites are blocked by specific anion adsorption from the supporting electrolyte, and consequently CO oxidation on Au(*hkl*) surfaces is more active in alkaline than in acid solution.

5. Conclusions

The electrooxidation of CO has been studied on reconstructed gold single-crystal surfaces by a combination of electrochemical and infrared reflection absorption spectroscopy measurements. Emphasis is placed on linking the microscopic vibrational properties of the CO adlayer to the voltammetric and other macroscopic electrochemical responses, including using rotating disk electrode measurements for determining the true catalytic activity of Au single-crystal surfaces. There are four significant new pieces of information provided by the IRAS/EC results that help us to gain insight into the interaction/kinetics of CO with reconstructed gold single-crystal surfaces.

The first observation is that the C−O stretching frequency on Au(*hkl*) is sensitive to the geometry of the adsorption site and can be observed in the range of 1940−1990 cm^{-1} for the 3-fold bridging, 2005−2070 cm^{-1} for the 2-fold bridging, and 2115−2140 for the terminal position. By comparison with Pt single-crystal surfaces, the C−O frequency bands on Au(*hkl*) give rise to a substantially higher (50−200 cm^{-1}) C−O frequency under the same experimental conditions attributed to a much weaker Au−CO interaction (i.e., the chemical shift effect).

The second characteristic is that the intensities as well as the morphology of the CO spectra are strongly dependent on the surface orientation. In contrast to previous findings, integrated intensities of both the 2-fold bridging C−O bands on Au(100)-"hex" and the 3-fold bridging C−O bands on Au(110)-(1 × 2) are comparable to the band intensities of CO adsorbed on Pt(100)-(1 × 1) and Pt(111)-(1 × 1).

The third characteristic is that, in "argon-purged" solution, the terminal CO band on Au(110)-(1 × 2) and the 3-fold CO bridge band disappear entirely. We have proposed that the disappearance of the C−O stretching band can be caused either by the oxidation of irreversibly adsorbed CO and/or by the reversible desorption of CO_{ad}.

The fourth characteristic is that the rate of CO oxidation varies with the crystal phase, with the activity of Au(110)-(1 × 2) and Au(100)-"hex" being higher than that for Au(111)-(1 × 23). It has been proposed that the observed structure sensitive rate of the CO oxidation reaction is controlled by the structure sensitive competitive adsorption of OH_{ad} and spectator species for the active (low-coordination) sites.

Acknowledgment. This work was supported by the Director, Office of Science, Office of Basic Energy Sciences, Division of Materials Sciences, U.S. Department of Energy under Contract No. DE-AC03-76SF00098. M.A. acknowledges the A. v. Humboldt Foundation for a Feodor−Lynen scholarship. The authors acknowledge C. A. Lucas for fruitful discussions.

(53) Verheij, L. K.; Hugenschmidt, M. B. *Surf. Sci.* **1998**, *416*, 37.

JA049038S